A Journal of the Gesellschaft Deutscher Chemiker

Angewandte International Edition Chemie

GDCh

www.angewandte.org

## Accepted Article

**Title:** Rational Crystalline Covalent Organic Frameworks Design for Efficient CO2 Photoreduction with H2O

**Authors:** Ya-Qian Lan, Meng Lu, Jiang Liu, Qiang Li, Mi Zhang, Ming Liu, Jin-Lan Wang, and Da-Qiang Yuan



**To be cited as:** *Angew. Chem. Int. Ed.* 10.1002/anie.201906890
*Angew. Chem.* 10.1002/ange.201906890

**Link to VoR:** http://dx.doi.org/10.1002/anie.201906890
http://dx.doi.org/10.1002/ange.201906890

WILEY-VCH

10.1002/anie.201906890


WILEY-VCH

# Rational Crystalline Covalent Organic Frameworks Design for Efficient $CO_2$ Photoreduction with $H_2O$

Meng Lu[1+], Jiang Liu[1+], Qiang Li[2], Mi Zhang[1], Ming Liu[1], Jin-Lan Wang[2], Da-Qiang Yuan[3], and Ya-Qian Lan[1,*]

Solar energy-driven conversion of $CO_2$ into fuels with $H_2O$ as sacrificial agent is still a challenging research field in photosynthesis. Here, a series of crystalline porphyrin-tetrathiafulvalene covalent organic frameworks (COFs) are synthesized and used as photocatalysts for reducing $CO_2$ with $H_2O$, in the absence of additional photosensitizer, sacrificial agent and noble metal co-catalyst. The effective photogenerated electrons transfer from tetrathiafulvalene to porphyrin by covalent bond, resulting in the separated electrons and holes respectively for $CO_2$ reduction and $H_2O$ oxidation. By adjusting the band structures of TTCOFs, TTCOF-Zn achieved the highest photocatalytic CO production of 12.33 μmol with ~100 % selectivity, along with $H_2O$ oxidation to $O_2$. Furthermore, density function theory calculations combined with the crystal structure model confirmed the structure-function relationship. Our work provides a new sight for designing more efficient artificial crystalline photocatalysts.

Excessive emission of carbon dioxide ($CO_2$) from fossil fuel burning into the atmosphere has caused severe energy and environmental issues that are urgent to be solved[1]. It is well-known that the significance of plant photosynthesis lies in that its ability to convert $CO_2$ with $H_2O$ into carbohydrate and $O_2$ by sunlight in a green manner. Consequently, artificial photosynthesis is expected to mimic above process efficiently for reducing $CO_2$ with $H_2O$ as electron donor, that is, integrating $CO_2$ reduction reaction ($CO_2$RR) and $H_2O$ oxidation half-reactions in one catalytic system, in which the development of photocatalysts is the most crucial factor[2]. However, it is a daunting work to enable these two half-reactions to couple and interact effectively. At present, only very limited strategies on the design of efficient photocatalyst can realize the overall reaction, such as Z-scheme heterojunction, yet they still face many problems.[3] Therefore, it is essential and pressing to explore new photocatalytic system with unambiguous structure for conducting photosynthetic overall reaction so as to obtain more insights into the structure-function relationship and then promote the development of this field.

Crystalline porous materials can provide a favorable structure-function research platform (including catalytic active site, charge transfer and reaction mechanism, etc.) for artificial photosynthesis because their well-defined structures can be elaborately designed and constructed by selecting appropriate building blocks or structural components according to specific demands.[4] Nevertheless, the majority of crystalline porous materials assembled with coordination bonds such as metal-organic frameworks (MOFs), few of them strong enough for performing the overall reaction (i.e. reducing $CO_2$ with $H_2O$ as electron donor).[5] By contrast, covalent organic frameworks (COFs) with directional structural designability, highly structural and chemical stabilities are a class of more promising porous crystalline materials for artificial photosynthesis[6]. Additionally, it is revealed that COFs with robust structure are able to afford permanent platform for catalytic active site[7] as well as large surface areas to fix $CO_2$[8], and their ordered π-array structures can provide pre-organized pathways for high-rate charge-carrier transport through delicate design[9]. Taking these considerations into account, it is feasible to build a multifunctional COFs photocatalyst system where the integration of $CO_2$ reduction and $H_2O$ oxidation half-reactions can be implemented. Unfortunately, to the best of our knowledge, few such system has been investigated in crystalline COF materials field up to now[10].

Herein, a series of crystalline 2D rigid porphyrin-tetrathiafulvalene COFs (TTCOF-M, M = 2H, Zn, Ni, Cu) were designed for artificial photosynthesis including $CO_2$ reduction and $H_2O$ oxidation. Electron-deficient metalloporphyrin (TAPP) complexes are known to have good visible-light collecting ability and potential $CO_2$ reduction performance[11], while electron-rich tetrathiafulvalene (TTF) molecule has proven to be a superior electron donor with rapid electron transfer[12]. Therefore, the effective covalent coupling between TAPP and TTF within COFs enables the visible-light driven electrons to efficiently separate and transfer from TTF to TAPP moiety, resulting in that the photoexcited electrons (on porphyrin) and holes (on TTF) can be used for reduction and oxidation reactions, respectively. As expected, TTCOF-Zn/Cu owing to suitable photocatalytic redox potentials were successfully used for reducing $CO_2$ with $H_2O$ as electron donor, and TTCOF-Zn exhibited the highest CO production of 12.33 μmol and selectivity (~100%) combined with excellent durability under our experimental conditions. Moreover, the corresponding density function theory (DFT) calculations agreed with the experimental results, which also gave detailed explanations about charge carrier transfer process and photocatalytic reaction pathways.

TTCOF-M were synthesized by Schiff-base condensation between metallized 5,10,15,20-tetrakis (4-aminophenyl)-porphinato] (TAPP-M, M = 2H, Zn, Ni, Cu) and 2,3,6,7-Tetra (4-formylphenyl)-tetrathiafulvalene by solvothermal method (Fig 1a). The crystalline structures of TTCOF-M were determined by the powder X-ray diffraction (PXRD) characterizations combined with theoretically structural simulations by *Materials Studio version 7.0*. An orthorhombic *P*222 space group based on TTCOF-Zn was built and carried out Le Bail refinements of the PXRD patterns for full profile fitting against the proposed models, which provided a unit cell parameter of a = 31.5694 Å, b = 21.9744 Å and c = 5.0014 Å, α = β = γ =90°. The simulated PXRD pattern using AA stacking mode reproduced the experimentally observed curve while AB stacking not, as

[*] M. Lu,[+] Dr. J. Liu, [+] M. Zhang, M. Liu, Prof. Y. -Q. Lan*,
Jiangsu Collaborative Innovation Centre of Biomedical Functional Materials, School of Chemistry and Materials Science, Nanjing Normal University. No. 1, Wenyuan Road, Nanjing, 210023 (China)
E-mail: yqlan@njnu.edu.cn
[*] Dr. Q. Li, Prof. J. -L. Wang,
School of Physics, Southeast University, Nanjing 211189 (China)
[*] Prof. D. -Q. Yuan,
State Key Laboratory of Structural Chemistry Fujian Institute of Research on the Structure of Matter, Chinese Academy of Sciences, Fuzhou, 350002 (China)
[+] These authors contributed equally to this work.

revealed by difference plot, with unweighted-profile R factor (Rp) = 2.544% and weighted-profile R factor (Rwp) = 3.349%, suggesting the validity of the computational model (Fig 1b). TTCOF-Zn has intense PXRD peaks at 4.98, 5.60, 6.9, 9.8 and 11.66°, which can be assigned to the 110, 200, 210, 220 and 320 faces, respectively. More details and raw data are given in SI.

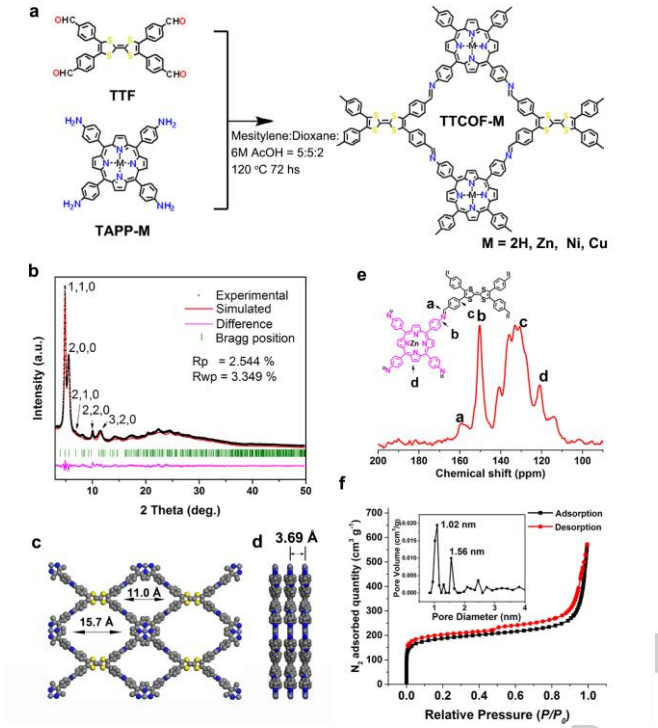


**Figure 1.** a) Schematic of the synthesis of TTCOF-M via the condensation of TTF and TAPP-M. b) Experimental (black dot) and simulated (red line) PXRD patterns of TTCOF-Zn c) Top and d) side views and e)$^{13}$C ssNMR spectrum of TTCOF-Zn. f) $N_2$ adsorption curve of TTCOF-Zn at 77 K (inset pore-size distribution profile).

These refinements finally revealed that there is a dual channel along c axis with theoretical pore sizes of 1.10 nm and 1.57 nm and pore volume of 0.94 cm$^3$/g (Fig 1c), and the distance between adjacent stacking 2D sheets is 3.69 Å (Fig 1d). Besides, TTCOF-2H/Ni/Cu also showed high crystallinity from their PXRD patterns (Fig S1-S3).

Fourier transform infrared spectroscopy (FTIR) and $^{13}$C solid-state nuclear magnetic resonance spectroscopy ($^{13}$C ssNMR) were used to confirm the chemical structure of TTCOF-M. From FTIR, the C=N stretching vibration band at 1620 cm$^{-1}$ appeared in the resultant TTCOF-M, while the C=O stretching vibration band at 1700 cm$^{-1}$ and -$NH_2$ vibration band at 3200~3500 cm$^{-1}$ belonged to reactant monomers that reduced obviously[13] (Fig S4-S5). Furthermore, the characteristic peak of ~158.9 ppm in $^{13}$C ssNMR corresponded to the carbon atom of the C=N bond[14] (Fig 1e and Fig S6-S7). These results confirmed the successful condensation reaction required for TTCOF-M structure. X-ray photoelectron spectroscopy (XPS) analysis results showed the divalent state of the central metal ion in porphyrin pocket of TTCOF-M (M = Zn, Ni, Cu) (Fig S8-S11).

The surface areas and porosity of TTCOF-M were determined by $N_2$ adsorption isotherms at 77 K (Fig 1f and Fig S12-S14). The Brunauer-Emmett-Teller (BET) surface area of TTCOF-Zn was calculated to be 564.6 m$^2$/g. Moreover, the total pore volume (0.93 cm$^3$/g) and the pore sizes (1.02 and 1.56 nm) for TTCOF-Zn are in conformity with theoretical calculation results. The chemical stability of TTCOF-Zn was examined by immersing it into different solvents at room temperature. The FTIR and PXRD patterns indicated its structural robustness (Fig S15-S16). The thermal stabilities of TTCOF-M were confirmed by thermogravimetric analysis (Fig S17-S20), which showed no obvious change up to 300 °C.

The morphology of TTCOF-M was characterized using scanning electron microscopy (SEM) and transmission electron microscopy (TEM), which shows that TTCOF-Zn is composed of hollow spheres with 1~3 μm in diameter and the self-assembled of small rectangular sheet-shaped crystals with about 0.1~0.2 μm in length (Fig 2a and Fig S21-S22). The fast Fourier transformation image of high-resolution transmission electron microscopy (HR-TEM) showed the hexagonal pore structure arrangement along the 001 crystal axis, which can also manifest the AA-stacking mode of 2D TTCOF-Zn structure (Fig 2b). Besides, energy-dispersive X-ray spectroscopy (EDS) analysis reveals that C, N, S and Zn elements are uniformly distributed over TTCOF-Zn (Fig S23-S25). The Zn content in TTCOF-Zn was determined to be ~4.3 wt % by inductively coupled plasma (ICP) optical emission spectrometry (Table S1).

The visible light-driven (420~800 nm) photocatalytic $CO_2$RR was conducted under pure $CO_2$ (1.0 atm, 298 K) atmosphere in $CO_2$ saturated $H_2O$ solution, without additional photosensitizer (PS) and sacrificial agents (SA). It is well known that the $CO_2$ absorption ability is an important factor for $CO_2$RR photocatalyst[15]. The $CO_2$ adsorption isotherms of TTCOFs were measured and determined to be 28, 52, 42 and 38 cm$^3$/g for TTCOF-2H/Zn/Ni/Cu, respectively (Fig 2c). The increased $CO_2$ adsorption capacity of TTCOF-Zn/Ni/Cu compared to the host TTCOF-2H should be attributed to the strong affinity between the metal ion and $CO_2$ molecule[16]. At the same time, water vapor adsorption tests for TTCOFs showed characteristic type II isotherm (Fig S26-S29), which indicated that the internal pore structure and external surface of these materials are accessible to water[17]. This hydrophilicity fact can also be demonstrated by water contact angles tests showing angle of 22-45° (Fig S.30).

Previous studies have revealed that to achieve photocatalytic $CO_2$RR with $H_2O$, the photocatalyst is required to have a more negative conduction band minimum (CBM) potential than $CO_2$ reduction potential ($CO/CO_2$, theoretically -0.53 V vs NHE, pH = 7 and -4.37 eV vs $E_v$, vacuum level) as well as more positive valence band maximum (VBM) potential than $H_2O$ oxidation potential ($O_2/H_2O$, theoretically 0.82 V vs NHE, pH = 7 and -5.67 eV vs $E_v$) [2b]. UV–vis diffuse reflectance spectroscopy (DRS) associated with ultraviolet photoelectron spectroscopy (UPS) were conducted to determine the electronic properties of TTCOF-M. These TTCOFs exhibited a broad visible-light absorption range, and the corresponding bandgaps ($E_g$) were determined to be 1.15, 1.49, 1.33 and 1.39 eV for TTCOF-2H/Zn/Ni/Cu by tauc-plots (Fig 2d inset and Fig S31-S33), respectively, suggesting the characteristics of semiconductor[18]. The VBM of TTCOF-Zn was calculated to be -5.76 eV (vs. $E_v$) from UPS pattern (Fig 2e) and the CBM was thus calculated to be -4.27 eV (vs. $E_v$). Mott–Schottky measurements were also conducted to determine the band positions of TTCOF-M (Fig S36), which were consistent with the results extracted from UPS. It is obvious that the CBM of TTCOF-Zn is more negative than the standard reduction potential of $CO/CO_2$ and its VBM is more positive than the oxidation potential of $O_2/H_2O$, suggesting its capability of integrating $CO_2$ reduction with $H_2O$ oxidation reactions. Similarly, the electronic properties of other COFs and COF-366-Zn was also obtained by the above mentioned

methods (Fig S34-S35 and S37-S44) and the energy-band alignment results were presented in Fig 2f. As we can see, TTCOF-Zn/Cu owing to the matched band structure fulfilled the artificial photosynthesis with $H_2O$ oxidation, while TTCOF-Ni and COF-366-Zn were considered to be unsuitable.

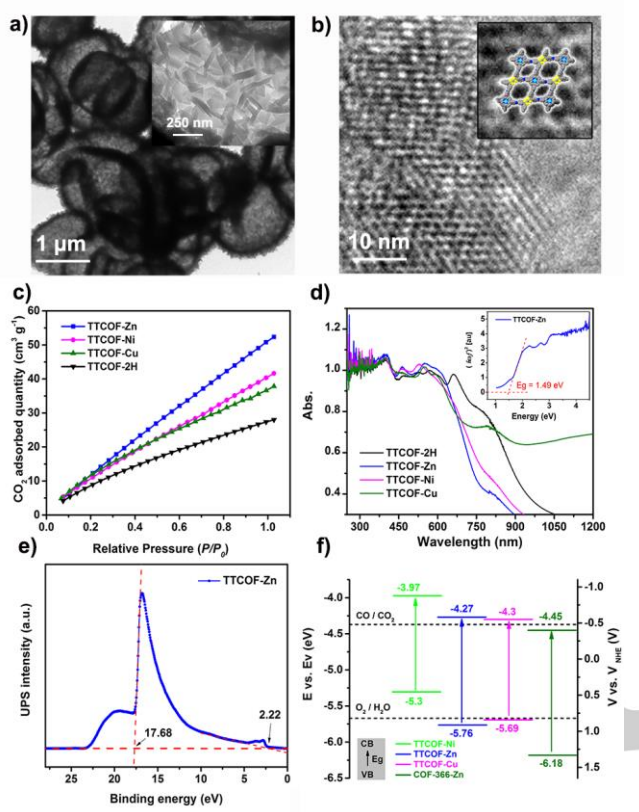


**Figure 2.** a) TEM images and b) HRTEM image of TTCOF-Zn, inset the pores are highlighted. c) $CO_2$ adsorption curves of TTCOF-M measured at 298 K. d) Solid-state UV-vis spectra of TTCOF-M. e) UPS spectra of TTCOF-Zn. f) Band structure diagram for TTCOF-M and COF-366-Zn.

The photocatalytic reactions were first carried out with TAPP-M monomers, no observable product was detected. When TTCOFs were used as photocatalysts, TTCOF-Zn showed the highest CO evolution of 12.33 μmol under visible light illumination after 60 hours, which was higher than that of TTCOF-Cu (8.65 μmol) and TTCOF-Ni (0.462 μmol) (Fig 3a, black). Each data is an average of three separate trials performed under the same conditions, and the standard deviation of these measurements is indicated by the error bar. At the same time, the yield of $O_2$ was also detected (Fig 3a and Fig S45-46). As expected, the CO: $O_2$ ratio is about 2:1. We can see that only the formed COFs exhibit prominent photocatalytic activity, and the mechanisms behind are discussed below. Moreover, the time-dependent CO output increased almost linearly with irradiation time for TTCOF-Zn as catalyst (Fig 3b). To further confirm the photocatalytic activity of TTCOFs, a series of control experiments were performed (Table S2). These results showed that no other gaseous products (except CO and $O_2$) were detected by gas chromatography (GC), while unquantifiable liquid composition was detected by $^1$HNMR (Fig S48), suggesting its high CO selectivity. The isotope labeling experiments were performed to ascertain the carbon and oxygen sources of photochemical products. Firstly we use $^{13}CO_2$ as substrates, $^{13}CO$ ($m/z$ = 29) was finally detected by using mass spectroscopy, which confirmed that the produced CO was originated from the reactant $CO_2$ instead of decomposition of catalyst (Fig 3c and Fig S49-50). Moreover, when $H_2{}^{18}O$ was used as reaction solution, $^{18}O_2$ ($m/z$ = 36) and $^{18}O^{16}O$ ($m/z$ = 34) were detected in the gas phase after the reaction (Fig S51), confirming that the generated $^{18}O_2$ stemmed from the oxidation of $H_2{}^{18}O$. Additionally, the photocatalytic durability of our catalyst system can maintain at least five cycles (Fig 3d). The crystallinity and structural integrity of TTCOF-Zn were retained after the reaction, as confirmed by PXRD, FTIR and XPS characterizations (Fig S52-S54). All of these evidences confirmed that TTCOF-Zn materials are efficient and selective heterogeneous photocatalysts for combining $CO_2$ photoreduction with $H_2O$ photooxidation.

Many characterization methods were performed to investigate the reasons for the different performances of these photocatalysts. Incident-photon-to-current conversion efficiency (IPCE) analysis was used to examine the photoinduced electron transfer (PET) efficiency. This results showed that the photo-current responses for TTCOF-Ms (metalloporphyrin) are much stronger than that of TTCOF-2H (metal-free) (Fig S55), indicating a more efficient separation of photogenerated electron-hole pairs by ligand-to-metal charge transfer effect. Besides, photoluminescence (PL) and time-resolved fluorescence decay techniques were further conducted to investigate the charge separation behaviors. The PL intensity

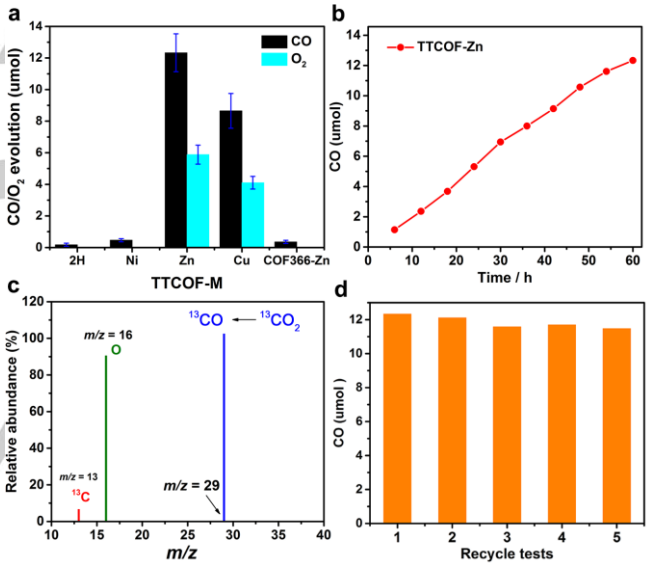


**Figure 3.** a) $CO_2$RR performances of TTCOF-M and COF366-Zn. b) time-dependent CO production performance by using TTCOF-Zn as photocatalyst c) MS of $^{13}CO$ produced from the photocatalytic reduction of $^{13}CO_2$. d) Durability tests of TTCOF-Zn.

of TTCOF-Zn was significantly quenched (Fig S56) compared to molecular TAPP-Zn and TTF. At the same time, TTCOF-Zn has a longer fluorescence lifetime ($\tau_1$ = 53.45 ± 1.6 ns) than that of TAPP-Zn (45.57 ± 0.76 ns) (Fig S57-S58), suggesting that the efficient electron transfer within COF is favorable for the promotion of charge separation efficiency.

Based on the above experiments and analysis, an intrinsic mechanism was proposed to explain the $CO_2$RR process with $H_2O$ oxidation: under the drive of visible-light irradiation, the PET process takes place from the TTF moiety (HOMO center) to the TAPP moiety (LUMO center) after absorbing photons, the excited electrons then move to catalytically active sites (Zn/Cu in TAPP) and used for $CO_2$ reduction. Meanwhile, the photogenerated holes in TTF are capable of oxidizing $H_2O$ to $O_2$, by which the catalytic system gains electrons from $H_2O$ to keep charge balance (Fig 4a).

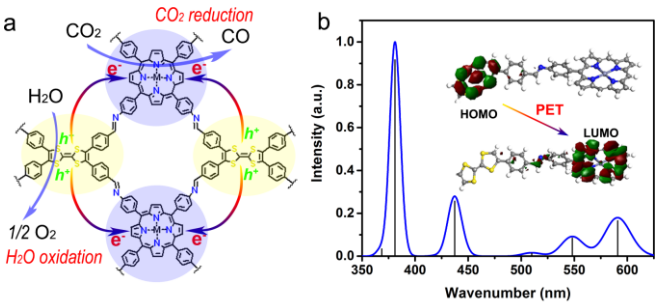


**Figure 4.** a) Schematic of the mechanism of TTCOF-M $CO_2$RR with $H_2O$ oxidation. b) Theoretical simulation UV−vis DRS of TTCOF-Zn and inset scheme PET route under light excitation.

Density functional theory (DFT) calculation study were applied to understand the photo-excitation process and catalytic reaction mechanisms. The low-lying electronic transitions in the TTCOF framework are shown in Fig 4b, and the insert demonstrates the first excitation contribution, i.e. from HOMO to LUMO. As we expected, the well-known electron donating TTF fragment dominates HOMO while LUMO is mainly contributed by TAPP part. Therein, the PET process can be readily occurred by light irradiation, which further forms photogenerated electrons located on the TAPP-M (formed TAPP-$M^-$) and photogenerated holes centered at the TTF unit (formed $TTF^+$). For the hole-doped $TTF^+$, the spin density mostly locates on linker C=C and the S atoms (Fig S59), indicating that the $H_2O$ oxidation process can be conducted on both sites. For the electrons located TAPP-$M^-$, the $CO_2$ reduction reaction will conduct on metal ion center. This result confirmed the above mechanism we proposed.

In summary, a series of 2D COFs were synthesized and used as photocatalysts to reduce $CO_2$ with $H_2O$ as electron donor, without additional PS, SA and noble metal co-catalyst. Thanks to the effective covalent coupling between porphyrin and tetrathiafulvalene molecules within TTCOFs, the electron-hole pairs induced by visible-light irradiation can be separated and transferred efficiently for $CO_2$ reduction and $H_2O$ oxidation reactions. TTCOF-Zn shows the highest photocatalytic CO production of 12.33 μmol with ~100 % selectivity and superior durability under our experimental conditions. This is the first report of rational designed crystalline COF system applied for selective photoreduction of $CO_2$ with $H_2O$ as electron donor. Moreover, we offering more straightforward and clearer crystalline evidence over the structure-function relationship of heterogeneous photocatalysts. Our research provides a new insight in designing next generation crystalline photocatalysts for artificial photosynthesis of $CO_2$ with $H_2O$.

## Acknowledgments

This work was financially supported by NSFC [No. 21622104, 21471080, 2170010097 and 21701085, BK20171032]; the NSF of Jiangsu Province of China [No. SBK2017040708]; the Natural Science Research of Jiangsu Higher Education Institutions of China [No. 17KJB150025]; Priority Academic Program Development of Jiangsu Higher Education Institutions and the Foundation of Jiangsu Collaborative Innovation Center of Biomedical Functional Materials.

**Keywords:** covalent organic frameworks • $CO_2$ photoreduction • $H_2O$ photooxidation • electron transfer

[1] a) J. Barber, P. D. Tran, *J. R. Soc. Interface* **2013**, *10*, 20120984; b) S. J. Davis, K. Caldeira, H. D. Matthews, *Science* **2010**, *329*, 1330-1333.
[2] a) X. Chang, T. Wang, J. Gong, *Energy Environ. Sci.* **2016**, *9*, 2177-2196; b) X. Liu, S. Inagaki, J. Gong, *Angew. Chem. Int. Ed.* **2016**, *55*, 14924-14950.
[3] a) K. Maeda, *ACS Catal.* **2013**, *3*, 1486-1503; b) H. Li, W. Tu, Y. Zhou, Z. Zou, *Advanced Science* **2016**, *3*, 1500389.
[4] a) S. Das, P. Heasman, T. Ben, S. Qiu, *Chem. Rev.* **2017**, *117*, 1515-1563; b) Y. Zhang, J. Duan, D. Ma, P. Li, S. Li, H. Li, J. Zhou, X. Ma, X. Feng, B. Wang, *Angew. Chem. Int. Ed.* **2017**, *56*, 16313-16317.
[5] N. C. Burtch, H. Jasuja, K. S. Walton, *Chem. Rev.* **2014**, *114*, 10575-10612.
[6] N. Huang, P. Wang, D. Jiang, *Nat. Rev.Mater.* **2016**, *1*, 16068.
[7] a) S. Lin, C. S. Diercks, Y. B. Zhang, N. Kornienko, E. M. Nichols, Y. Zhao, A. R. Paris, D. Kim, P. Yang, O. M. Yaghi, C. J. Chang, *Science* **2015**, *349*, 1208-1213; b) S. Yang, W. Hu, X. Zhang, P. He, B. Pattengale, C. Liu, M. Cendejas, I. Hermans, X. Zhang, J. Zhang, J. Huang, *J. Am. Chem. Soc.* **2018**, *140*, 14614-14618.
[8] A. Nagai, Z. Guo, X. Feng, S. Jin, X. Chen, X. Ding, D. Jiang, *Nat. Commun.* **2011**, *2*.
[9] S. Wan, F. Gándara, A. Asano, H. Furukawa, A. Saeki, S. K. Dey, L. Liao, M. W. Ambrogio, Y. Y. Botros, X. Duan, S. Seki, J. F. Stoddart, O. M. Yaghi, *Chem. Mater.* **2011**, *23*, 4094-4097.
[10] a) S. Yang, W. Hu, X. Zhang, P. He, B. Pattengale, C. Liu, M. Cendejas, I. Hermans, X. Zhang, J. Zhang, J. Huang, *J. Am. Chem. Soc.* **2018**; b) Y. Fu, X. Zhu, L. Huang, X. Zhang, F. Zhang, W. Zhu, *Applied Catalysis B: Environmental* **2018**, *239*, 46-51.
[11] a) T. Kojima, T. Honda, K. Ohkubo, M. Shiro, T. Kusukawa, T. Fukuda, N. Kobayashi, S. Fukuzumi, *Angewandte Chemie-International Edition* **2008**, *47*, 6712-6716; b) K. Kilsa, J. Kajanus, A. N. Macpherson, J. Martensson, B. Albinsson, *J. Am. Chem. Soc.* **2001**, *123*, 3069-3080.
[12] a) C. M. Davis, Y. Kawashima, K. Ohkubo, J. M. Lim, D. Kim, S. Fukuzumi, J. L. Sessler, *J. Phys. Chem. C.* **2014**, *118*, 13503-13513; b) A. Jana, S. Bahring, M. Ishida, S. Goeb, D. Canevet, M. Salle, J. O. Jeppesen, J. L. Sessler, *Chem. Soc. Rev.* **2018**, *47*, 5614-5645; c) C. K. Graetzel, M. Graetzel, *The Journal of Physical Chemistry* **1982**, *86*, 2710-2714.
[13] P. Shao, J. Li, F. Chen, L. Ma, Q. Li, M. Zhang, J. Zhou, A. Yin, X. Feng, B. Wang, *Angew. Chem.* **2018**, *130*, 16739-16743.
[14] S. Y. Ding, J. Gao, Q. Wang, Y. Zhang, W. G. Song, C. Y. Su, W. Wang, *J. Am. Chem. Soc.* **2011**, *133*, 19816-19822.
[15] H. Zhang, J. Wei, J. Dong, G. Liu, L. Shi, P. An, G. Zhao, J. Kong, X. Wang, X. Meng, *Angew. Chem. Int. Ed.* **2016**, *55*, 14310-14314.
[16] a) H.-Q. Xu, J. Hu, D. Wang, Z. Li, Q. Zhang, Y. Luo, S.-H. Yu, H.-L. Jiang, *J. Am. Chem. Soc.* **2015**, *137*, 13440-13443; b) S. Li, Y. Dong, J. Zhou, Y. Liu, J. Wang, X. Gao, Y. Han, P. Qi, B. Wang, *Energy & Environmental Science.* **2018**, *11*, 1318-1325.
[17] X. Wang, L. Chen, S. Y. Chong, M. A. Little, Y. Wu, W.-H. Zhu, R. Clowes, Y. Yan, M. A. Zwijnenburg, R. S. Sprick, A. I. Cooper, *Nat. Chem.* **2018**, *10*, 1180-1189.
[18] G. Zhang, Z. A. Lan, L. Lin, S. Lin, X. Wang, *Chem. Sci.* **2016**, *7*, 3062-3066.

10.1002/anie.201906890


WILEY-VCH

# COMMUNICATION

Text for Table of Contents

A series crystalline covalent organic frameworks were designed and applied for $CO_2$ photoreduction coupled with $H_2O$ photooxidation, with the absence of any photosensitizer and sacrificial agent, giving more straightforward and clear understanding over the structure-function relationship of artificial photosynthesis.

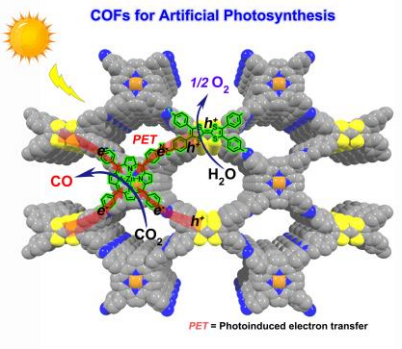


*Meng Lu, Jiang Liu, Qiang Li, Mi Zhang, Ming Liu, Jin-Lan Wang, Da-Qiang Yuan, and Ya-Qian Lan**

***Page No. – Page No.***

**Rational Crystalline Covalent Organic Frameworks Design for Efficient $CO_2$ Photoreduction with $H_2O$**